Available online at www.sciencedirect.com

SciVerse ScienceDirect

Ceramics International 39 (2013) 6591–6598

CERAMICS INTERNATIONAL

www.elsevier.com/locate/ceramint

The effect of iron incorporation on the *in vitro* bioactivity and drug release of mesoporous bioactive glasses

Ying Zhang[a,b], Yu Liu[a], Mingzhong Li[a,*], Shenzhou Lu[a], Jiannan Wang[a]

[a]*National Engineering Laboratory for Modern Silk, College of Textile and Clothing Engineering, Soochow University, Suzhou 215123, People's Republic of China*

[b]*Inorganic Materials Department, College of Chemistry, Chemical Engineering and Materials Science, Soochow University, Suzhou 215123, People's Republic of China*

Received 20 December 2012; received in revised form 25 January 2013; accepted 25 January 2013
Available online 1 February 2013

Abstract

Magnetic mesoporous bioactive glasses with the composition xFe–$(80-x)SiO_2$–15CaO–$5P_2O_5$ (mol%) (Fe/MBGs) were prepared by the non-ionic block copolymer $EO_{20}PO_{70}EO_{20}$ (P123) surfactant as template and the evaporation-induced self-assembly process using Ca, P, Si and Fe sources. The structure, morphology and magnetic properties of Fe/MBGs were characterized by X-ray diffraction, scanning electron microscopy, infrared spectra, vibrating sample magnetometer and N_2 adsorption–desorption technique. The results show that Fe/MBGs have porous network (pore diameter of 50–100 nm), mesoporous walls (mesoporous size of 4–5 nm), and that the mesostructure, magnetic properties and *in vitro* bioactivity of the Fe/MBGs depend on the chemical composition. Furthermore, the Fe incorporation in the MBGs enhanced the magnetic properties, demonstrated sustained drug delivery and maintained apatite-formation ability in SBF. This means that the Fe/MBGs allowed bioactivity could improve their drug delivery capacity, thus enhancing their potential applications as bioactive filler materials for bone tissue regeneration.

Keywords: Magnetic property; Mesoporous bioactive glasses; Iron; Drug delivery

1. Introduction

The applications of mesoporous bioactive glasses (MBGs) scaffolds as protein/drug carriers and bone filling materials have drawn growing interest in recent years [1–3]. Compared with non-mesoporous bioglasses scaffolds, MBGs scaffolds have much more optimal surface area and pore volume, as evidenced by its greatly enhanced drug delivery capability, *in vitro* apatite mineralization and degradation [4,5]. For those reasons, most researchers pay attention to the preparation and application of 3D porous MBGs scaffolds in bone tissue engineering and the drug delivery system [6–8], and generally believe that 3D porous scaffolds provide more advantages to repair large bone defects than the other shapes of MBGs materials [9,10]. Meanwhile, experiments show that the other shapes of MBGs materials, such as the magnetic MBGs powders, also have a capacity to improve the *in vitro* apatite mineralization and degradation, and can be applied to the bone tissue engineering and the drug delivery system [11,12]. Compared with traditional macroporous scaffolds, the main advantage of the magnetic MBGs powders is that they possess not only better drug-delivering properties, but also the ability to fill bone defects of irregular and complex shapes and sizes [13,14].

Combining the MBGs with magnetic nanoparticles (such as Fe_3O_4 and Fe_2O_3) is of great interest for drug delivery [15,16]. They can carry the drugs and be guided to the targeted organs or locations inside the body, which will facilitate the therapeutic efficiency and avoid the damage of normal organs or tissues resulted from the drug toxicity before targeting the desired positions. Obviously, Fe ions play an important role in the functioning of the body that an appropriate content of iron ions effectively enhance bone metabolism, especially osteoblastic proliferation, differentiation, and calcification [17]. We hypothesized that incorporating Fe ions into the MBGs

*Corresponding author. Tel./fax: +86 512 65880089.
E-mail address: mzli@suda.edu.cn (M. Li).

0272-8842/$ - see front matter © 2013 Elsevier Ltd and Techna Group S.r.l. All rights reserved.
http://dx.doi.org/10.1016/j.ceramint.2013.01.094

would make it magnetic properties, and at the same time, influence its mesoporous structure and biological properties. Therefore, the principal aim of this study was to incorporate Fe ions into the MBGs to control their drug loading and release properties. For this purpose, Fe^{3+} as a substitute for Si^{4+} in the MBGs structure was prepared and the effects of Fe ions on the mesoporous structure and *in vitro* biological properties of Fe/MBGs materials were elucidated.

2. Experimental procedures

2.1. Preparation of Fe/MBGs

The Fe incorporated MBGs (xFe–$(80-x)SiO_2$–15CaO–$5P_2O_5$ (mol%)) were prepared by incorporating 3%, 6% or 9% Fe into MBGs through a sol–gel method [6]. The chemical composition and amounts of reagents used to prepare the Fe/MBGs are listed in Table 1. In a typical synthesis for the 6Fe/MBGs, 4.0 g of P123 (M_w=5800, Sigma), 6.1 g of tetraethyl orthosilicate (TEOS, 98%, Sigma), 1.4 g of calcium nitrate (Ca $(NO_3)_2 \cdot 4H_2O$), 0.38 g of ferric chloride ($FeCl_3$), 0.73 g of triethyl phosphate (TEP, 99.8%, Sigma) and 1.0 g 0.5 M HCl were dissolved in 60 g of ethanol and stirred at room temperature for 1 day. The resulting sol was introduced into a petri dish for an evaporation-induced self-assembly process, and then the dry gel was calcined at 700° C for 5 h to obtain 6Fe/MBGs. Others were prepared by the same method except for their Fe content.

2.2. Characterization of Fe/MBGs

The X-ray diffraction (SAXRD and WAXRD) of samples was examined on the X-ray diffractometer (XRD, Model D/MAX-III, Japan) using Cu Kα radiation (λ=1.5406 Å) and the detective range from 0.5° to 70°. The morphology of samples was inspected on the field-emission scanning electron microscope (SEM, S-4800, Japan). Fourier transform infrared spectra were determined with the infrared spectrophotometer (FT-IR, Nicolet 5700, American) operated at a resolution of 2 cm^{-1}. Brunauer–Emmett–Teller and Barret–Joyner–Halenda analyses were used to determine the specific surface area, the nanopore size distribution and the pore volume from N_2 adsorption–desorption isotherms. Magnetic measurements were carried out at room temperature using the vibrating sample magnetometer (VSM, BHV-55, Japan) with a maximum magnetic field of 20000 Oe.

2.3. In vitro bioactivity of the Fe/MBGs in SBF

The assessment of apatite-mineralization ability of the Fe/MBGs was carried out in SBF solution, which was prepared and buffered at pH 7.4 with tris (hydroxymethyl) aminomethane $[(CH_2OH)_3CNH_2]$ and hydrochloric acid (HCl) according to Kokubo and Takadama [18]. Generally, 0.1 g of the powders was soaked in 100 mL of SBF solution in a polyethylene bottle at 37° C for 1, 3 and 7 days, with stirring at 160 rpm. After soaking, the Fe/MBGs were collected from SBF solution, rinsed with ethanol and dried naturally. XRD, SEM and FTIR analyses were used to study the evolution of the surface of the Fe/MBGs.

2.4. Drug loading and in vitro release of aspirin from Fe/MBGs

Aspirin (Sigma, 99%) served as a model drug, was dissolved in anhydrous ethanol. 1.0 g of the Fe/MBGs was added to 25 mL of aspirin anhydrous ethanol solution with a concentration of 40 mg/mL at room temperature [19]. The vials were sealed to prevent the evaporation of ethanol, and the mixture was then stirred for 24 h. The products were filtered and dried at 60° C. The samples were named as Fe/MBGs–aspirin. The filtrate was extracted from the vial and analyzed by UV/vis spectroscopy at a wavelength of 268 nm.

0.1 g of the Fe/MBGs–aspirin was immersed into 100 mL of phosphate buffer silane (PBS, pH 7.0) at 37° C, with stirring at 100 rpm for 3, 6, 9, 25, 49, 73, 97, 121 and 169 h. The release medium (5.0 mL) of the sample was removed for analysis at given time intervals using a syringe and replaced with the same volume of fresh preheated PBS. The extracted medium was analyzed by UV/vis spectroscopy at a wavelength of 268 nm. The cumulative release of aspirin (%) was calculated using the equation: aspirin (%)=(total amount of aspirin released/ total loading amount of aspirin loaded) × 100%.

3. Results and discussion

3.1. Characterization of as-prepared Fe/MBGs

In the sol–gel process, using ethanol as phase separation solvent, the Fe incorporated MBGs was synthesized. Fig. 1 shows the representative SEM images of as-prepared Fe/MBGs. The samples 0Fe/MBGs, 3Fe/MBGs, 6Fe/MBGs

Table 1
Chemical composition and amounts of reagents for preparation of the Fe/MBGs.

Samples	Ca/P/Fe/Si molar ratio	P123 (g)	$Ca(NO_3)_2 \cdot 4H_2O$ (g)	TEP (g)	$FeCl_3$ (g)	TEOS (g)
0Fe/MBGs	15/5/0/80	4	1.4	0.73	0	6.70
3Fe/MBGs	15/5/3/77	4	1.4	0.73	0.19	6.34
6Fe/MBGs	15/5/6/74	4	1.4	0.73	0.38	6.10
9Fe/MBGs	15/5/9/71	4	1.4	0.73	0.57	5.85

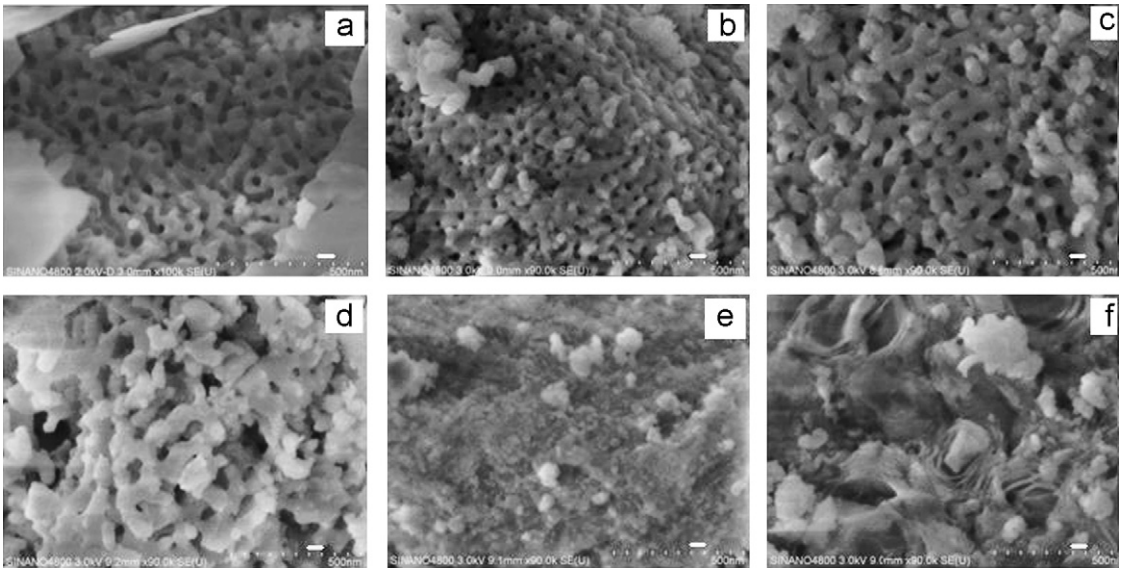

Fig. 1. SEM images of as-prepared Fe/MBGs. Scale bar: (a)–(f) for 50 nm. (a) 0Fe/MBGs; (b) 3Fe/MBGs; (c) 6Fe/MBGs; (d) 9Fe/MBGs; (e) 12Fe/MBGs; and (f) 15Fe/MBGs.

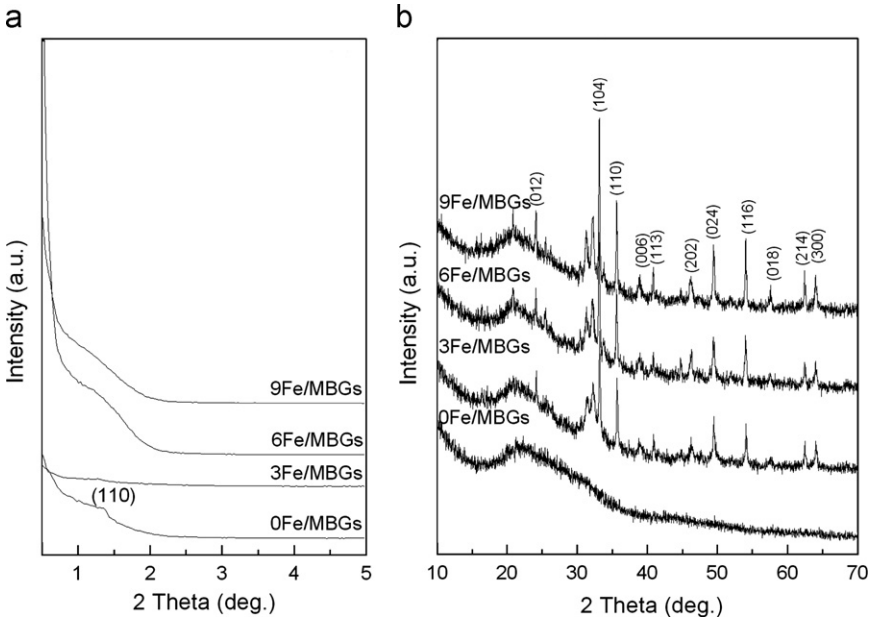

Fig. 2. Small angle (a) and wide angle (b) XRD patterns for as-prepared MBGs with different Fe contents.

and 9Fe/MBGs all exhibited a porous structure with a similar small pore size range from 30 to 100 nm. But, this porous structure is not observed in the samples12Fe/MBGs and 15Fe/MBGs, indicating partial replacement of Si^{4+} in glass network with Fe^{3+} ions may disrupt the ordered orientation of SiO_4^{4-} during the self-assembly reaction, thus modifying the surface morphology. With an increase of Fe/Si mol ratios in MBGs, the mesoporous structure of bioactive glass may change or even disappear.

Fig. 2(a) shows the SAXRD patterns of as-prepared Fe/MBGs. The result shows that the diffraction peak located at around $2\theta = 1.25^\circ$ appears in the sample 0Fe/MBGs, indexed to the (110) diffractions of a two-dimensional hexagonal mesostructure. The peak then weakens with increasing Fe content, implying that the substitution (in part) of Fe^{3+} for Si^{4+} changes the ordered two-dimensional hexagonal mesostructure. It may be ascribed to the bonds in $[FeO_4]$ tetrahedron that is responsible for the imbalanced chemical interaction between the $[SiO_4]$ tetrahedron layers or within $[SiO_4]$ tetrahedron layers during MBGs formation, resulting in the mesoporous network would be easily destroyed. The WAXRD patterns of as-prepared Fe/MBGs are shown in Fig. 2(b). A broad reflection at $2\theta = 15$–30° associated with amorphous silicate can be noticed in all

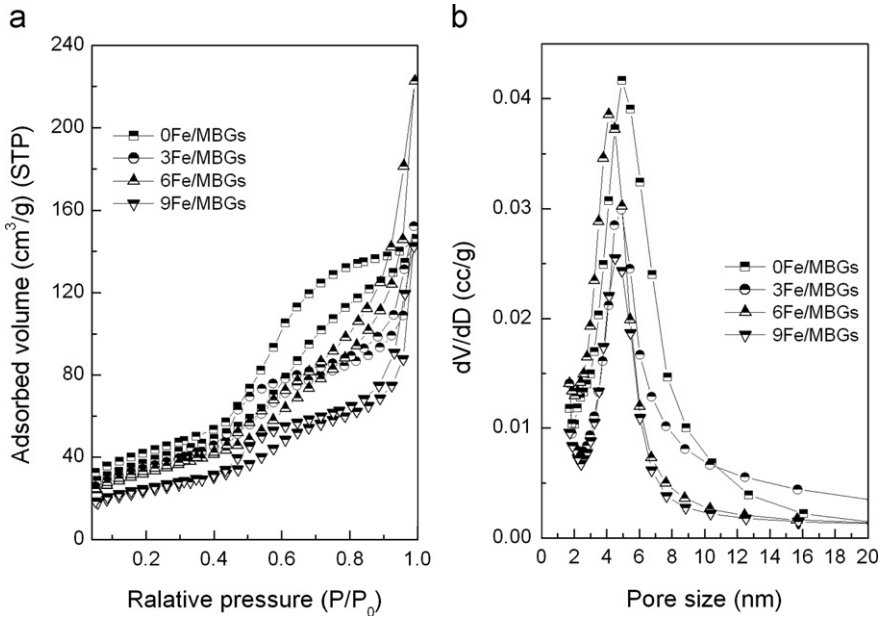

Fig. 3. N_2 adsorption–desorption isotherms (a) and the pore size distribution (b) of as-prepared Fe/MBGs.

Table 2
The structure parameters of as-prepared Fe/MBGs.

Samples	S_{BET} (m^2/g)	D_p (peak) (nm)
0Fe/MBGs	134	5
3Fe/MBGs	114	4.8
6Fe/MBGs	121	4.1
9Fe/MBGs	84	4.5

XRD patterns of 0Fe/MBGs, 3Fe/MBGs, 6Fe/MBGs and 9Fe/MBGs. Except for 0Fe/MBGs, other Fe/MBGs exhibited the diffraction peaks of Fe_2O_3 (JCPDS 03-0800) in Fig. 2(b). The position and relative intensity of diffraction peaks match well with the standard diffraction data of Fe_2O_3 powder, which indicated the Fe_2O_3 phase borned.

The results of N_2 adsorption–desorption analysis of as-prepared Fe/MBGs are shown in Fig. 3 and Table 2. The isotherm of Fe/MBGs can be classified as type IV isotherms characteristic of mesoporous materials, but it displays different hysteresis loop in the range of 0.98–1.0P/P_0. The 0Fe/MBGs exhibit a hysteresis loop of type H1, while other Fe/MBGs show a hysteresis loop of type H3. The corresponding pore size curves of Fe/MBGs show a narrow pore size distribution range from 4 to 5 nm. It was interesting to note that the mesoporous size was affected by the incorporation of Fe, decreasing from 5 nm (0Fe/MBGs) to 4.1 nm (6Fe/MBGs). BET analysis showed that the specific surface areas of the 0Fe/MBGs, 3Fe/MBGs, 6Fe/MBGs and 9Fe/MBGs were 134, 114, 121 and 84 $m^2\ g^{-1}$,respectively. Thus, it can be seen that mesoporous size and specific surface area of bioactive glass have been changed by the introduction of iron. While the sample 6Fe/MBGs has relatively higher specific surface area and smaller mesoporous size compared with the other samples doped with iron.

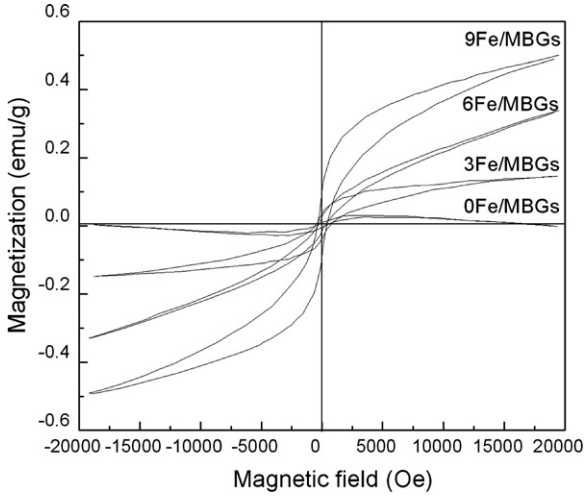

Fig. 4. The magnetic hysteresis loops of as-prepared Fe/MBGs.

Fig. 4 shows the magnetic hysteresis loops of the samples with different contents of Fe measured at room temperature. It was found from Fig. 4 that the Fe/MBGs exhibit a ferromagnetic behavior not a superparamagnetic behavior because of the formation of Fe_2O_3. The saturation magnetization of the samples increased with an increase of Fe content. 9Fe/MBGs had a more obvious hysteresis loop than the others.

3.2. *In vitro* bioactive of as-prepared Fe/MBGs in SBF

The bioactive characteristic of the MBGs is their ability to bond with living bone through the formation of an apatite layer on their surface both *in vitro* [20,21]. In this study, XRD, SEM and FTIR spectra were conducted to evaluate the apatite-mineralization ability of the Fe/

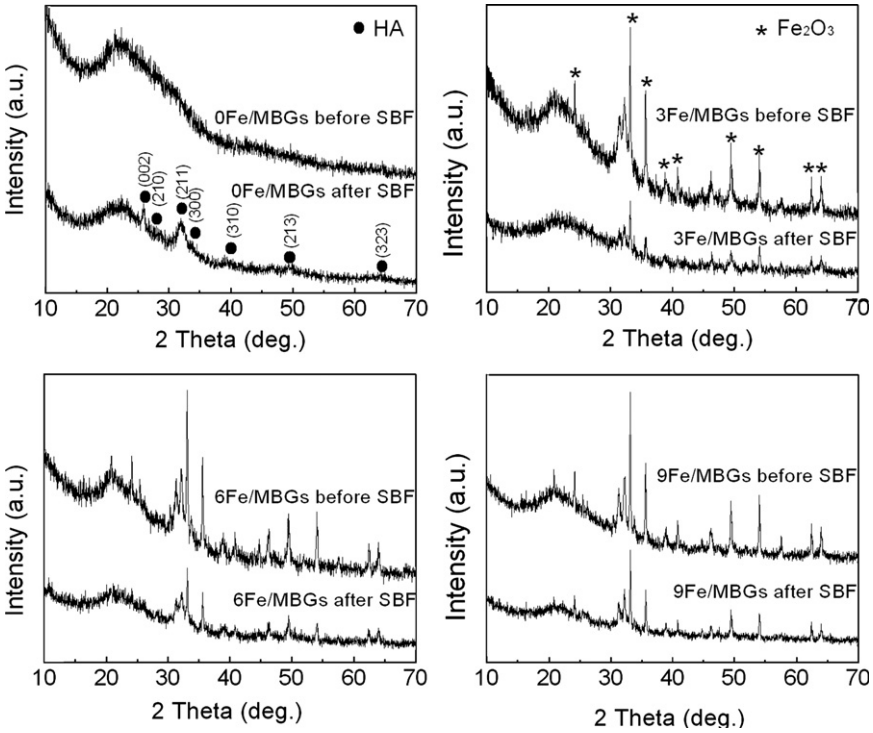

Fig.5. XRD patterns of as-prepared Fe/MBGs before and after soaking in SBF for 7 days.

MBGs. Fig. 5 shows the XRD patterns of as-prepared 0Fe/MBGs, 3Fe/MBGs, 6Fe/MBGs and 9Fe/MBGs before and after soaking in SBF solution at 37° C for 7 days. After 7 days, the presence of a broad reflection at $2\theta = 18–25°$ is due to the amorphous silicate. Noticeably, for sample 0Fe/MBGs after 7 days, the diffraction peaks at $2\theta = 25.9°$, 29.1°, 31.9°, 33.6°, 39.7°, 49.6° and 64.3° appear in the XRD pattern (Fig. 5), which can be assigned to the (002), (210), (211), (300), (310), (213) and (323) diffraction of crystalline apatite phase. This implies that sample 0Fe/MBGs already has good apatite-mineralization ability. While for other samples, the corresponding diffraction peaks of crystalline apatite phase were covered with diffraction peaks of crystalline Fe_2O_3 phase. It would be difficult to distinguish where the diffraction peaks of crystalline apatite phase were and whether the crystalline apatite phase formation occurs in the process of soaking in SBF solution at 37° C for 7 days. Nevertheless, it can still deduce that the mineral hydroxyapatite matrix might form from the decreased intensities of the diffraction peaks of Fe/MBGs.

Fig. 6 shows the SEM images of as-prepared 0Fe/MBGs, 3Fe/MBGs, 6Fe/MBGs and 9Fe/MBGs after soaking in SBF for 3 and 7 days. It can be observed that a layer composed of needle-shaped crystallites fully covered the surface of the sample 0Fe/MBGs during the soaking period. The MBGs with different Fe compositions still maintained the porous structure after 3 and 7 days soaking in SBF, and only the porosity of the surface decrease. It is hard to clearly observe the hydroxyl carbonate apatite layer on the surface of Fe/MBGs. The results show that the glass network connection degree of MBGs has been modified by the introduction of Fe with different amounts, in turn, influences the ability of the deposition of hydroxyl carbonate apatite in SBF.

Fig. 7 shows the FTIR spectra of as-prepared 0Fe/MBGs, 3Fe/MBGs, 6Fe/MBGs and 9Fe/MBGs before and after soaking in SBF for 7 days. The peaks at 1070, 789 and 467 cm^{-1} are assigned to the Si–O–Si vibration bands. After soaking in SBF solution for 7 days, the vibrational bands of hydroxyl carbonate apatite were detected besides the Si–O–Si bands. The vibrational peaks at 980 cm^{-1} assigned to C–O vibration bands, and the vibrational peaks at 606 and 567 cm^{-1} assigned to P–O vibration bands, can be clearly observed for all samples. While the vibrational peaks at 603 and 564 cm^{-1} assigned to Fe–O vibration bands can be distinctly observed only for the samples 3Fe/MBGs, 6Fe/MBGs and 9Fe/MBGs. Meanwhile, with the increase of the Fe content, the intensities of P–O vibrational peaks for the samples 3Fe/MBGs, 6Fe/MBGs and 9Fe/MBGs were much stronger than that of 0Fe/MBGs. This may owe to the superposition effect of characteristic peaks of Fe–O and P–O bands at 600–560 cm^{-1} wavenumber range.

3.3. Loading and in vitro release of aspirin from the Fe/MBGs

Drug delivery represents another major challenge for bioactive filler materials applicable for bone tissue engineering. In this study, aspirin was used as a model drug to monitor the drug loading and release kinetics of the Fe/MBGs. Aspirin, as a target drug, could potentially be

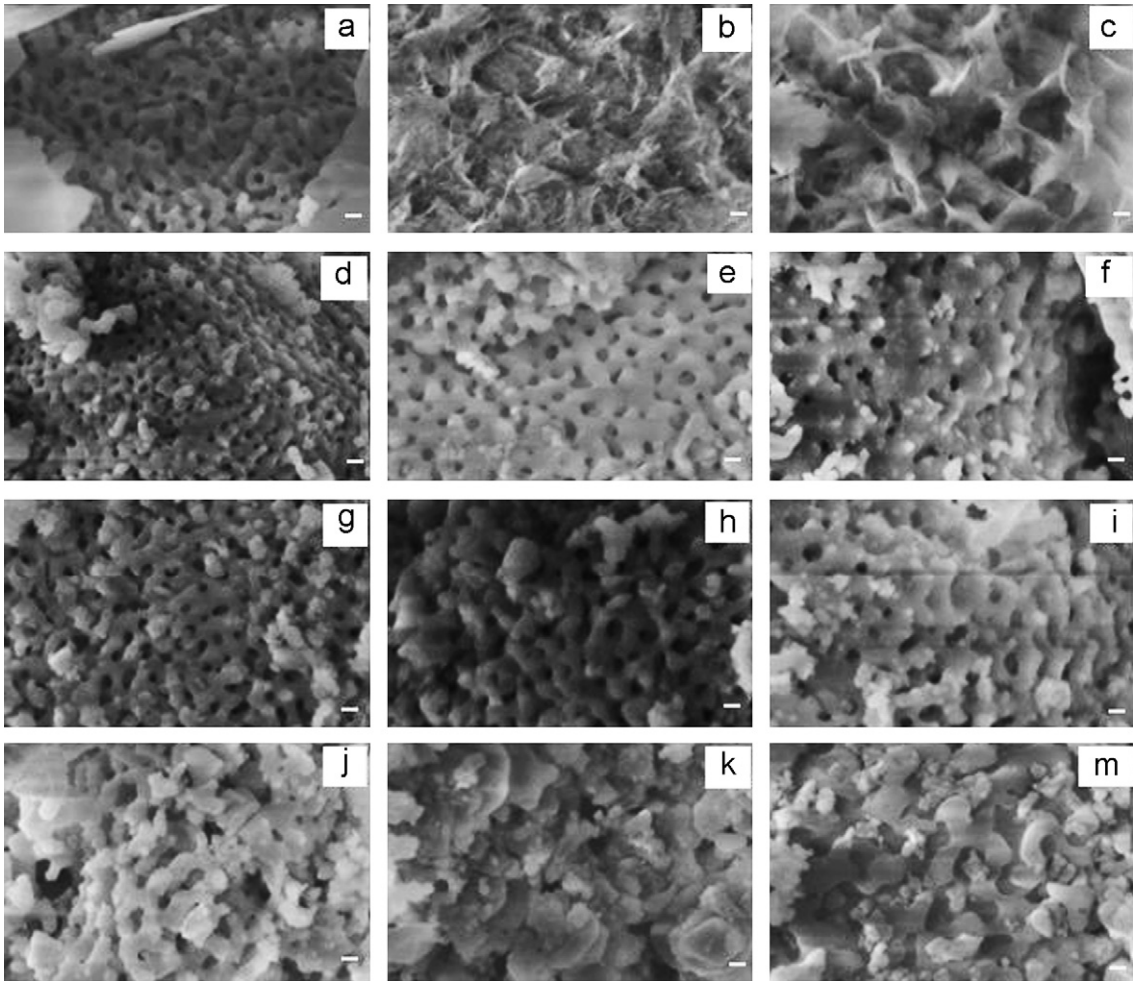

Fig. 6. SEM images of 0Fe/MBGs (a) before, (b) and (c) after; 3Fe/MBGs (d) before, (e) and (f) after; the 6Fe/MBGs (g) before, (h) and (i) after; the 9Fe/MBGs (j) before, (k) and (m) after, soaking in SBF for 3 and 7 days. Scale bar: (a)–(m) for 50 nm.

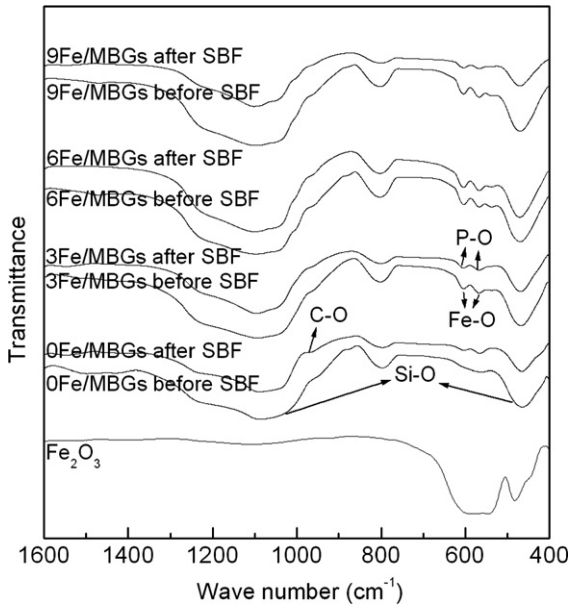

Fig. 7. FTIR spectra for as-prepared Fe/MBGs before and after soaking in SBF for 7 days.

applied in fracture repair to minimize inflammation by virtue of its anti-inflammatory function. Fig. 8 shows the typical FTIR spectra of aspirin and as-prepared 0Fe/MBGs before and after loading aspirin. After loading aspirin, the sample 0Fe/MBGs–aspirin shows bands at 1420, 1557 and 1585 cm^{-1} corresponding to the C–H bending vibration in the aspirin molecules. One band at 1756 cm^{-1} ascribed to carbonyl group of aspirin is still present on the spectrum, which also indicates that aspirin does not degrade. Therefore, it proves that aspirin has been loaded in the Fe/MBGs as well.

Fig. 9 shows the accumulative aspirin release from the samples 0Fe/MBGs, 3Fe/MBGs, 6Fe/MBGs and 9Fe/MBGs in PBS. It can be observed that all these samples presented a similar release behavior during the whole period, which is a two-step release behavior, an initial burst release followed by a relatively slow release. And the aspirin release from Fe/MBGs was slower in the first 12 h and the accumulative release of aspirin is lower for 7 days except the sample 3Fe/MBGs compared with sample undoped iron. The most likely explanation for this is that the partial replacement of Si^{4+} in glass network with Fe^{3+}

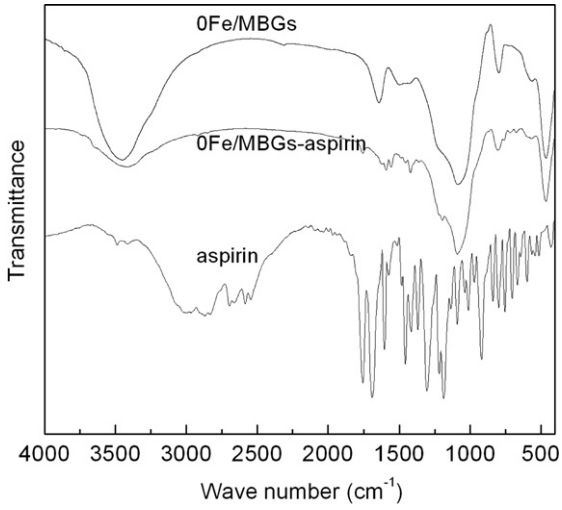

Fig. 8. FTIR spectra of aspirin and 0Fe/MBGs before and after loading aspirin.

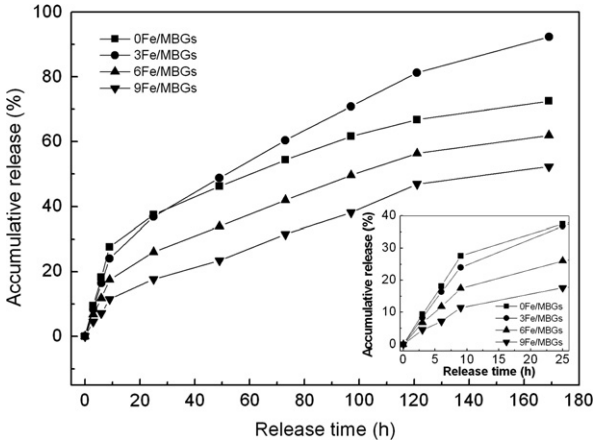

Fig. 9. Aspirin release from Fe/MBGs with different Fe contents.

ions would disrupt the ordered orientation of SiO_4^{4-}, or Fe ions in MBGs could form the second phase (Fe_2O_3) distributing on the grain boundary, which is possible to modify the mesoporous structure and slow the drug release. Therefore, the aspirin release can be controlled by controlling the contents of Fe in MBGs, and a higher Fe content would result in a slower release of aspirin (Fig. 9).

4. Discussion

The magnetic MBGs with different proportions of Fe ions have been prepared by a combination of P123 surfactant as co-templates and evaporation induced self-assembly process. The effects of Fe ions on the mesopore structure, magnetic properties, biological properties and drug delivery of MBGs have been investigated. Incorporating Fe into MBGs endowed them magnetic, as expected, improved their biological properties and, at the same time, had the capability of sustained drug delivery.

Magnetic MBGs would be used for the hyperthermia treatment to kill the diseased cells, which is prepared by replacing Si^{4+} with Fe^{3+} in the MBDs structure. The magnetic properties are provided by the MBGs components that increased with the increase of Fe content. The temperature required damaging or killing cancer cells is more than 42° C that depends on the magnetic field intensity of both the material and the external magnetic field [4,22]. This means adjusting Fe content could control the saturation magnetization of Fe/MBGs that is a very helpful way to control and create the temperature needed to destroy diseased cells. Therefore, the as-prepared Fe/MBGs with hyperthermia therapy and local drug release properties might be able to improve healing ability upon the bone disease compared with single therapy method.

To study the *in vitro* bioactivity of as-prepared Fe/MBGs, the apatite formation ability in SBF was investigated. From the results of XRD, SEM and FTIR, we can see the Fe contents play an important role to influence the apatite-mineralization ability of the Fe/MBGs in SBF. The needle-shaped apatite layer with a certain thickness could be formed on 0Fe/MBGs after soaking 3 and 7 days in SBF solution. Nevertheless, it is hard to clearly observe the apatite layer on the surface of Fe/MBGs with increasing the Fe content. Only the surface microstructure of Fe/MBGs was changed. According to the mechanism of apatite formation on the silicate bioactive glass, more Ca ions in SBF and more Si–OH groups on the silicate bioactive glass facilitate the apatite formation [23,24]. In this study, the Fe^{3+} ions replaced Si^{4+} ions in the Fe/MBGs, less Si–OH ions released from the Fe/MBGs with the increase of the Fe content, which may change the apatite formation on the surfaces of the Fe-incorporated MBGs. On the other hand, it also shows that the bioactive glass surface induced the formation of apatite are slower because of the Fe incorporating. However, the incorporation of Fe into MBG may be still an effective method to prepare magnetic bioactive composite materials.

The mesoporous structure is important for drug loading and delivery. Our data show that the mesoporous size and specific surface area of bioactive glass have been modified by the introduction of iron. The sample 6Fe/MBGs has a higher specific surface area (121 $m^2 g^{-1}$) and a smaller mesoporous size (4.1 nm) compared with the other samples doped with iron. The Fe ions, as a kind of modifier into the mesoporous glass network are positive correlation with its +3 valence and 4 coordination numbers, so a fraction of the Fe ions could occupy the core of tetrahedral sites. Based on the glass theory, the oxygen–silica ratio has been calculated. According to calculations, oxygen–silica ratios in the sample Fe/MBGs are lower than that in 0Fe/MBGs, indicating the number of bridging oxygen in the Fe/MBGs was higher than that in 0Fe/MBGs. The results show that the addition of Fe ions could strengthen the connection degree of the glass network and stimulate vitrification process. So, the mesoporous structures of Fe/MBGs are strongly modified by the Fe doping amount. Although the

incorporation (less than 9 percent) of Fe into MBGs partially changed the mesoporous structure, they still have a certain specific surface area, indicating that they have the ability to adsorb the drugs and subsequently maintain sustained release.

5. Conclusions

The Fe contained bioactive inorganic mesoporous glasses (Fe/MBGs) were prepared using a sol–gel method. The incorporation of Fe ions into MBGs plays an important role in influencing the mesoporous structure, magnetic and biological properties. In addition, the prepared Fe/MBGs maintain sustained drug delivery, which indicates that as-prepared Fe/MBGs have the potential as a targeted release material. This may be a effective way combine the magnetic properties with the advantage of bioactive inorganic mesoporous glass in the bone tissue engineering to treat bone disease. However, the sol–gel process affects the magnetic properties of Fe/MBGs. Magnetic measurements carried out in the Fe/MBGs showed that the maximum saturation magnetization at room temperature was 0.5 emu/g for an applied field of 20,000 Oe. Further studies will be conducted to investigate how to obtain a higher surface area, improve the magnetic properties of Fe/MBGs and observe their function of drug release with hyperthermia treatment for preventing and curing bone disease.

Acknowledgments

This research was supported by the Universities Natural Science Research Project of Jiangsu Province (11KJD430004) and the Project Funded by the Priority Academic Program Development of Jiangsu Higher Education Institution (PAPD).

References

[1] C.X. Gao, Q. Gao, X.X. Bao, Y.D. Li, A. Teramoto, K. Abe, Preparation and in vitro bioactivity of novel mesoporous borosilicate bioactive glass nanofibers, Journal of the American Ceramic Society 94 (2011) 2841–2845.

[2] N. Li, R.D. Wang, Macroporous sol–gel bioglasses scaffold with high compressive strength, porosity and specific surface area, Ceramics International 38 (2012) 6889–6893.

[3] X.P. Wang, X. Li, A. Ito, Y. Sogo, Synthesis and characterization of hierarchically macroporous and mesoporous $CaO–MO–SiO_2–P_2O_5$ (M = Mg, Zn, Sr) bioactive glass scaffolds, Acta Biomaterials 7 (2011) 3638–3644.

[4] C. Wu, W. Fan, Y. Zhu, M. Gelinsky, J. Chang, G. Cuniberti, V. Albrecht, T. Friis, Y. Xiao, Multifunctional magnetic mesoporous bioactive glass scaffolds with a hierarchical pore structure, Acta Biomaterials 7 (2011) 3563–3572.

[5] C. Wu, R. Miron, A. Sculean, S. Kaskel, T. Doert, R. Schulze, Y. Zhang, Proliferation, differentiation and gene expression of osteoblasts in boron-containing associated with dexamethasone deliver from mesoporous bioactive glass scaffolds, Biomaterials 32 (2011) 7068–7078.

[6] C. Wu, Y. Ramaswamy, Y. Zhu, R. Zheng, R. Appleyard, A. Howard, The effect of mesoporous bioactive glass on the physiochemical, biological and drug release properties of poly (DL-lactide-co-glycolide) films, Biomaterials 30 (2009) 2199–2208.

[7] S.J. Wang, H.S. Jain, High surface area nanomacroporous bioactive glass scaffold for hard tissue engineering, Journal of the American Ceramic Society 93 (2010) 3002–3005.

[8] B.S. Miguel, R. Kriauciunas, S. Tosatti, M. Ehrbar, C.G. Marcus, Enhanced osteoblastic activity and bone regeneration using surface-modified porous bioactive glass scaffolds, Journal of Biomedical Materials Research Part A 94 (2010) 1023–1033.

[9] B. Francesco, V.B. Chiara, Three-dimensional glass-derived scaffolds for bone tissue engineering: current trends and forecasts for the future, Journal of Biomedical Materials Research Part A 97 (2011) 514–535.

[10] M.B. Coelho, M.M. Pereira, Sol–gel synthesis of bioactive glass scaffolds for tissue engineering: effect of surfactant type and concentration, Journal of Biomedical Materials Research Part B 75 (2005) 451–456.

[11] M. Zhu, J.L. Shi, Q.J. He, L.X. Zhang, F. Chen, An emulsification-solvent evaporation route to mesoporous bioactive glass microspheres for bisphosphonate drug delivery, Journal of Materials Science 47 (2012) 2256–2263.

[12] B. Lei, X.F. Chen, Y.J. Wang, N.R. Zhao, C. Du, L.M. Fang, Synthesis and bioactive properties of macroporous nanoscale $SiO_2–CaO–P_2O_5$ bioactive glass, Journal of Non-Crystalline Solids 355 (2009) 2678–2681.

[13] F.Y. Hsu, S.C. Chueh, Y.J. Wang, Microspheres of hydroxyapatite/reconstituted collagen as supports for osteoblast cell growth, Biomaterials 20 (1999) 1931–1936.

[14] M. Alcaide, P. Portolés, A. López-Noriega, D. Arcos, M. Vallet-Regí, M.T. Portolés, Interaction of an ordered mesoporous bioactive glasses with osteoblasts, fibroblasts and lymphocytes, demonstrating its biocompatibility as a potential bone graft material, Acta Biomaterials 6 (2010) 892–899.

[15] X. Li, X.P. Wang, Z.L. Hua, J.L. Shi, One-pot synthesis of magnetic and mesoporous bioactive glass composites and their sustained drug release property, Acta Materialia 56 (2008) 3260–3265.

[16] Joseph M. Kinsella, S. Ananda, Jennifer S. Andrew, Joel F. Grondek, M.P. Chien, M. Scadeng, Nathan C. Gianneschi, E. Ruoslahti, Michael J. Sailor, Enhanced magnetic resonance contrast of Fe_3O_4 nanoparticles trapped in a porous silicon nanoparticle host, Advanced Materials 23 (2011) H248–H253.

[17] K. Yamasaki, H. Hagiwara, Excess iron inhibits osteoblast metabolism, Toxicology Letters 191 (2009) 211–215.

[18] T. Kokubo, H. Takadama, How useful is SBF in predicting in vivo bone bioactivity, Biomaterials 27 (2006) 2907–2915.

[19] Y. Zhu, E. Kockrick, T. Ikoma, N. Hanagata, S. Kaskel, An efficient route to rattle-type $Fe_3O_4@SiO_2$ hollow mesoporous spheres using colloidal carbon spheres templates, Chemistry of Materials 21 (2009) 2547–2553.

[20] G.F. Wei, X.X. Yan, J. Yi, L.Z. Zhao, L. Zhou, Y.H. Wang, C.Z. Yu, Synthesis and in-vitro bioactivity of mesoporous bioactive glasses with tunable macropores, Microporous and Mesoporous Materials 143 (2011) 157–165.

[21] C.J. Shih, H.T. Chen, L.F. Huang, P.S. Lu, H.F. Chang, I.L. Chang, Synthesis and in vitro bioactivity of mesoporous bioactive glass scaffolds, Materials Science and Engineering C 30 (2010) 657–663.

[22] T.W. Wang, H.C. Wu, W.R. Wang, F.H. Lin, P.J. Lou, M.J. Shieh, The development of magnetic degradable DP-Bioglass for hyperthermia cancer therapy, Journal of Biomedical Materials Research Part A 83 (2007) 828–837.

[23] L.L. Hench, J. Wilson, Surface-active biomaterials, Science 226 (1984) 630–636.

[24] C. Cerruti, N. Sahai, Silicate biomaterials for orthopaedic and dental implants, Reviews in Mineralogy & Geochemistry 64 (2006) 283–313.